

*Chapter 2***MECHANICS OF ORIGIN OF FLOW LIQUEFACTION
INSTABILITY UNDER PROPORTIONAL STRAIN TRIAXIAL
COMPRESSION**

- [1] U. Mital and J.E. Andrade. “Mechanics of origin of flow liquefaction instability under proportional strain triaxial compression”. In: *Acta Geotechnica* (2016), pp. 1–11. doi: [10.1007/s11440-015-0430-8](https://doi.org/10.1007/s11440-015-0430-8). URL: <http://link.springer.com/article/10.1007/s11440-015-0430-8/fulltext.html>.

2.1 Introduction

Liquefaction is a field-scale phenomenon, typically associated with earthquake-induced shaking, that causes a loss of strength of saturated cohesionless granular media. It can lead to catastrophes such as landslides, tilting and settlement of buildings, and failure of dams, bridges, and retaining walls [27]. Typically, liquefaction can be divided into flow liquefaction and cyclic mobility [27, 44]. The US National Academy of Science’s National Research Council [27] defined flow liquefaction as, “the condition where a soil mass can deform continuously under a shear stress less than or equal to the static shear stress applied to it.” Flow liquefaction is the more devastating manifestation of liquefaction that can lead to field-scale catastrophes. Cyclic mobility, on the other hand, is a more benign form of liquefaction which does not lead to loss of stability.

Although primarily associated with earthquakes, flow liquefaction has been shown to occur under both static and dynamic loading [36, 44, 48, 79]. It occurs when the shear stress required for static equilibrium of a soil mass is greater than the shear strength of the soil in its liquefied state [44]. Given its consequences, it is important to not only understand this phenomenon, but also what causes it in the first place. Although progress has been made in understanding the macro and micro mechanics at the onset of flow liquefaction instability [3, 19, 20, 22, 42, 66], our understanding of the *origin* of this phenomenon is still incomplete. For instance, why are loose sands susceptible to flow liquefaction under undrained conditions [44]? How much increase in pore pressure is sufficient to induce liquefaction, and why does

the amount vary under different initial conditions [44]?. In addition, it is usual to assume that flow liquefaction instability occurs under completely undrained or constant volume conditions. However, there is evidence [27, 53, 69, 84] to suggest that soil may undergo volume changes during earthquake shaking. Under static loading, a soil may be experiencing volume changes due to unequal pore pressure generation in adjacent soil layers of different densities [80, 84]. Flow liquefaction under such conditions cannot be attributed to constant volume deformations. Our central objective is to address the aforementioned issues by investigating the origins of flow liquefaction instability under proportional strain triaxial compression conditions.

We start by defining a flow liquefaction potential for determining flow liquefaction susceptibility during proportional strain triaxial compression. A proportional strain triaxial test is one in which the imposed volume change (or the imposed dilatancy) is proportional to the axial strain on the soil specimen. If the volume is imposed to be constant (isochoric strain compression), then the test becomes an undrained triaxial test [21]. The flow liquefaction potential is a function of inconsistency between the natural dilative tendency of the soil and the imposed dilatancy during proportional strain triaxial compression. Such a potential has been used previously [21]. Previous works also imply that [19–22, 42] that given the right conditions, a loose soil that contracts during drained triaxial compression and liquefies under undrained triaxial compression may be stable under proportional strain triaxial compression. Conversely, a dense soil that dilates during drained triaxial compression and is stable under undrained triaxial compression may liquefy under proportional strain triaxial compression. The undrained loose case is a special case of proportional strain triaxial compression under which a soil can liquefy. By analyzing the defined flow liquefaction potential, we provide an interpretation about the micro-mechanics at play which make a soil susceptible to flow liquefaction. Furthermore, we also analyze stress evolution during proportional strain triaxial compression and discuss the mechanics of the test leading up to flow liquefaction instability. We arrive at a necessary precursor for instability, which can serve as a warning sign for flow liquefaction instability under proportional strain triaxial compression, whilst the soil is still stable. It is important to note that the precursor is not a condition of sufficiency and should also not be confused with the onset of instability itself. The same loading must be applied continuously to induce flow liquefaction instability. This provides further insight into the mechanics of origin of flow liquefaction instability under proportional strain triaxial compression.

2.2 Soil response under proportional strain triaxial compression

In a proportional strain triaxial compression test, the volumetric strain increment is proportional to the axial strain increment. The undrained triaxial compression test is a special case where the proportion is equal to zero, resulting in a constant volume test. The behavior of soil under proportional strain triaxial compression can be either ‘stable’ or ‘unstable’. Figure 2.1 presents a typical response of soil under proportional strain triaxial compression conditions.

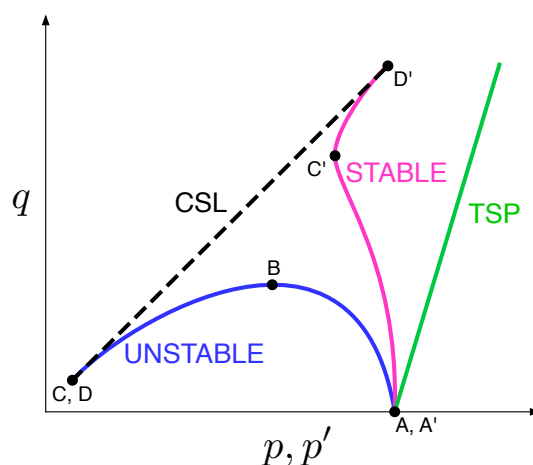


Figure 2.1: Effective stress paths of stable and unstable sands under proportional strain triaxial compression. The total stress path (TSP) and critical state line (CSL) are also sketched for reference. A = start, B = Instability, C = phase transformation, D = critical state. In unstable sands, points C and D are often indistinguishable [36]. A', C', and D' are the corresponding points in a stable sand.

Instability or *unstable* behavior is characterized by loss of deviatoric strength when a soil is subjected to deviatoric strain increments. In case of an undrained triaxial test on a loose sand, this loss of deviatoric strength coincides with the vanishing of second order work, which has been shown to be associated with bursts in kinetic energy and extensive strain softening [19, 22]. This is accompanied by a large pore pressure build up. Under proportional strain triaxial conditions, however, loss of deviatoric strength and vanishing of second order work do not necessarily coincide. To that effect, some investigators have proposed an alternate response parameter whose peak coincides with the vanishing of second order work [19, 20, 22, 42]. In any case, experimental and numerical results of the aforementioned investigators also suggest that along with the vanishing of second order work, loss of deviatoric strength is also a necessary condition for flow liquefaction under proportional strain conditions in a triaxial test. We will briefly discuss the alternate response parameter

in section 2.4. Presently, for the sake of simplicity, we consider the deviatoric stress as a response parameter in our work. Once the soil specimen reaches the peak in effective stress space (characterized by peaking of deviatoric stress), it advances to flow liquefaction failure, assuming that the same loading path is applied continuously. Therefore, a necessary condition for unstable flow liquefaction behavior can be expressed as:

$$\dot{q} < 0 \quad (2.1)$$

where \dot{q} is the deviatoric invariant of the stress rate tensor.

In case of *stable* behavior, the soil specimen may initially exhibit behavior reminiscent of a loose sand under undrained triaxial compression. However, before the soil specimen reaches the peak in effective stress space, it undergoes a phenomenon called ‘phase transformation’ [36], whereby it starts exhibiting behavior reminiscent of a dilative sand under undrained triaxial compression. This phenomenon ostensibly provides stability, whereby the pore water pressure build-up and strain softening are kept in check.

In what follows, $\dot{\sigma}$ is the stress increment tensor and $\dot{\epsilon}$ is the strain increment tensor. We use subscripts a and r to denote the axial and radial components respectively. $\dot{p} = (\dot{\sigma}_a + 2\dot{\sigma}_r)/3$ and $\dot{q} = (\dot{\sigma}_a - \dot{\sigma}_r)$ are the volumetric and deviatoric invariants of stress increment ($\dot{\sigma}$), respectively. $\dot{\epsilon}_v = (\dot{\epsilon}_a + 2\dot{\epsilon}_r)$, and $\dot{\epsilon}_s = 2(\dot{\epsilon}_a - \dot{\epsilon}_r)/3$ are the volumetric and deviatoric invariants of strain increment ($\dot{\epsilon}$), respectively.

2.3 Flow Liquefaction Potential

In order to determine whether the behavior of a soil specimen under proportional strain triaxial compression will be stable or unstable, we define a *flow liquefaction potential* \mathcal{L} . For a soil to be susceptible to unstable flow liquefaction behavior, we postulate that:

$$\mathcal{L} > 0 \quad (2.2)$$

Conversely, for stable soil behavior, we postulate that $\mathcal{L} < 0$. The condition when $\mathcal{L} = 0$ will be discussed later. We define the functional form of \mathcal{L} as:

$$\mathcal{L} = \beta - \beta_p \quad (2.3)$$

where β is the *natural dilative tendency* of the soil specimen, and β_p is the *imposed dilatancy* on the specimen during proportional strain triaxial compression. *Natural*

dilatative tendency may be defined as the volume change that a soil specimen must undergo such that pore pressure does not evolve. The natural dilatative tendency of a soil specimen can be determined from its behavior under fully drained conditions. A soil that contracts during drained triaxial compression has $\beta > 0$, while a soil that dilates during drained triaxial compression has $\beta < 0$. On the other hand, *imposed dilatancy* is the volume change *imposed* on a soil specimen during a proportional strain triaxial test, which is normally different from the natural dilatative tendency and leads to an evolution in pore pressure. Equation 2.3 is similar to a liquefaction potential defined by Darve and Pal [21]. While Darve and Pal [21] derived the potential using ideas from continuum plasticity, it will become apparent that our potential has been derived by considering imposed radial strain increments.

Mathematically, natural dilatative tendency β can be defined as [85]:

$$\beta = \frac{\dot{\epsilon}_v}{\dot{\epsilon}_s} \quad (2.4)$$

where we have assumed elastic strain increments to be negligible. We define imposed dilatancy β_p as:

$$\beta_p = \frac{\dot{\epsilon}_v^p}{\dot{\epsilon}_s^p} \quad (2.5)$$

where the superscript p denotes imposed proportional strain triaxial compression. Note that for imposed dilatancy, we are concerned with total strain increments.

We now take a closer look at drained and proportional strain triaxial compression in order to understand why $\mathcal{L} > 0$ makes a soil susceptible to flow liquefaction instability.

Drained Triaxial Compression

Drainage of pore water ensures that pore pressures do not evolve. It also implies that the granular assembly undergoes changes in volume. Using the definition of β , volumetric strain increment $\dot{\epsilon}_v$ can be expressed as a function of shear strain increment $\dot{\epsilon}_s$:

$$\dot{\epsilon}_v = \beta \dot{\epsilon}_s \quad (2.6)$$

Using the definitions of $\dot{\epsilon}_v$ and $\dot{\epsilon}_s$ from section 2.2, we can obtain the radial strain increment $\dot{\epsilon}_r$ consistent with the natural dilatative tendency of the assembly, given an

applied axial strain increment $\dot{\epsilon}_a$:

$$\dot{\epsilon}_r = \alpha \dot{\epsilon}_a =: \dot{\epsilon}_r^d \quad (2.7)$$

where α is function of natural dilative tendency β :

$$\alpha = \frac{2\beta - 3}{2\beta + 6} \quad (2.8)$$

Note that $\alpha < 0$. This is because soil has a positive poisson's ratio, implying that compressing the granular assembly in the axial direction will make it expand or stretch out in the radial direction. We have assumed the usual geomechanics convention of compression being positive.

Proportional Strain Triaxial Compression

However, in a proportional strain triaxial compression test, the volumetric strain increment $\dot{\epsilon}_v$ is constrained to be proportional to the axial strain increment $\dot{\epsilon}_a$. Equivalently, we may say that given an applied axial strain increment $\dot{\epsilon}_a$, the radial strain increment $\dot{\epsilon}_r$ is:

$$\dot{\epsilon}_r = \alpha_p \dot{\epsilon}_a =: \dot{\epsilon}_r^p \quad (2.9)$$

where α_p may or may not be constant. For simplicity, it is often imposed as a constant. It may be noted that α_p is similar to R defined in literature [19–22, 42]. Several investigators have devised experimental programs whereby for axisymmetric conditions prevalent in a triaxial test, such strain paths can be imposed [15, 19, 80]. For a saturated sample, volume changes imposed during such strain paths can be associated with injection or extraction of water in the soil sample [20], such that the drainage is incompatible with that during a drained test, leading to pore pressure variation. Such a test has also been referred to as a partially drained test in the past [80].

In any case, the relation between α_p and β_p is same as the relation between α and β (equation 2.8). Therefore, by inverting equation 2.8, the imposed dilatancy β_p can be obtained as a function of α_p :

$$\beta_p = \frac{3(1 + 2\alpha_p)}{2(1 - \alpha_p)} \quad (2.10)$$

The undrained test is a special case where $\alpha_p = -1/2$, yielding $\beta_p = 0$.

We are now in a position to understand how the flow liquefaction potential \mathcal{L} can help in evaluating flow liquefaction susceptibility of a soil subjected to proportional strain triaxial compression. Using equation 2.10, \mathcal{L} can be expressed as a function of α and α_p :

$$\mathcal{L} = \frac{9(\alpha - \alpha_p)}{2(1 - \alpha)(1 - \alpha_p)} \quad (2.11)$$

Note that a positive poisson's ratio implies $\alpha < 0$. In addition, proportional strain triaxial compression tests are conducted such that $\alpha_p < 0$. Therefore, the denominator in equation 2.11 above is a positive quantity. This means that:

$$\text{sign}(\mathcal{L}) = \text{sign}(\alpha - \alpha_p) \quad (2.12)$$

Equivalently, since both α and α_p are negative:

$$\boxed{\text{sign}(\mathcal{L}) = \text{sign}(|\alpha_p| - |\alpha|)} \quad (2.13)$$

For a soil to be susceptible to flow liquefaction during proportional strain triaxial compression, we postulated that $\mathcal{L} > 0$. This implies that given an axial strain increment $\dot{\epsilon}_a$, the radial strain increments for proportional $\dot{\epsilon}_r^p$ and drained $\dot{\epsilon}_r^d$ triaxial compression are related as:

$$|\dot{\epsilon}_r^p| > |\dot{\epsilon}_r^d| \quad (2.14)$$

where we have used equations 2.7 and 2.9. Equation 2.14 implies that the imposed proportional radial strain increment is more expansive than the drained radial strain increment. Micro-mechanically, this may be interpreted as soil grains pushing outwards and spreading more intensely than the natural dilative tendency. This increases the load on pore water, causing pore water pressure to rise during proportional strain triaxial compression, making the assembly susceptible to flow liquefaction.

Conversely, for a soil to exhibit stable behavior during proportional strain triaxial compression, we postulated that $\mathcal{L} < 0$. This implies that given an axial strain increment $\dot{\epsilon}_a$, the radial strain increments for proportional ($\dot{\epsilon}_r^p$) and drained ($\dot{\epsilon}_r^d$) triaxial compression are related as:

$$|\dot{\epsilon}_r^p| < |\dot{\epsilon}_r^d| \quad (2.15)$$

Equation 2.15 implies that the imposed proportional radial strain increment is less expansive than the drained radial strain increment. Micro-mechanically, this may

be interpreted as soil grains pushing outwards less intensely than the natural dilative tendency. The grains tend to coalesce together, creating a pulling or suction effect on the pore water, that causes pore water pressure to fall during proportional strain triaxial compression, making the assembly stable. See Figure 2.2 for a cartoon of the discrepancy in radial strain increments for both $\mathcal{L} > 0$ and $\mathcal{L} < 0$.

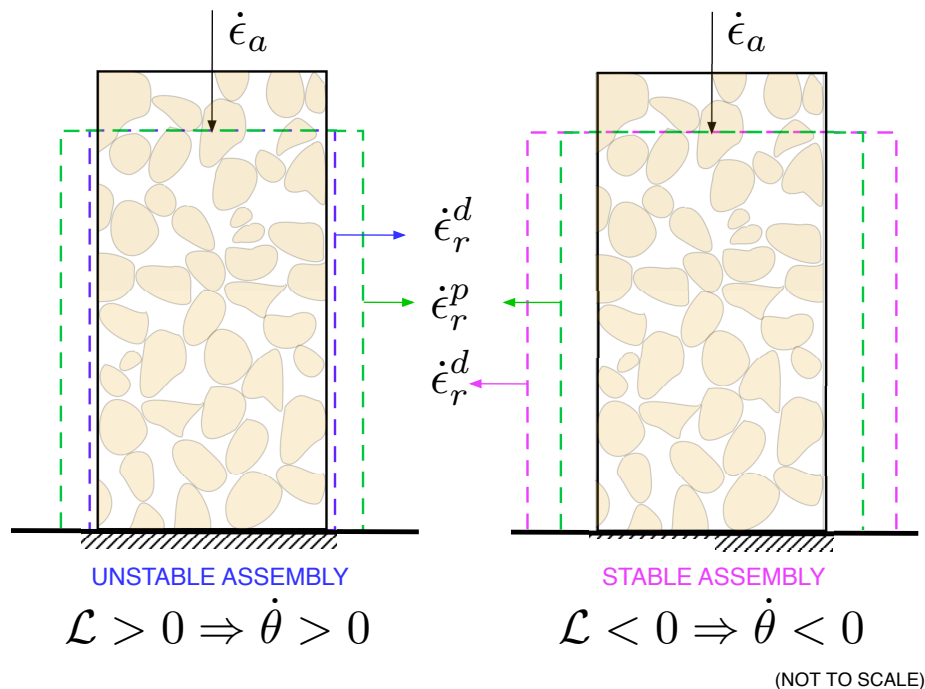


Figure 2.2: Cartoon showing the mismatch between the imposed proportional ($\dot{\epsilon}_r^p$) and the drained ($\dot{\epsilon}_r^d$) radial strain increments, given an axial strain increment ($\dot{\epsilon}_a$). In an unstable assembly, $\mathcal{L} > 0$, which means that the imposed radial strain increments are more expansive than the natural dilative tendency. As a result, soil grains push outward and spread more intensely than the natural dilative tendency. This increases the load on pore water, causing pore water pressure to rise ($\dot{\theta} > 0$). Conversely, for a stable assembly, $\mathcal{L} < 0$, which means that soil grains push outwards less intensely than the natural dilative tendency. The grains tend to coalesce together, creating a pulling or suction effect on the pore water, which causes pore water pressure to fall ($\dot{\theta} < 0$).

Undrained Triaxial Compression

As we mentioned earlier, undrained triaxial compression is a special case of proportional strain triaxial compression where $\beta_p = 0$, implying $\mathcal{L} = \beta$. Therefore, a soil that contracts during drained triaxial compression ($\beta > 0$) is susceptible to flow liquefaction under undrained triaxial compression, whereas a soil that dilates dur-

ing drained triaxial compression ($\beta < 0$) exhibits stable behavior under undrained triaxial compression.

Discussion

It is important to note that given the right conditions, a loose soil that contracts during drained triaxial compression and liquefies under undrained triaxial compression may be stable under proportional strain triaxial compression. Conversely, a dense soil that dilates during drained triaxial compression and is stable under undrained triaxial compression, may liquefy under proportional strain triaxial compression. Such loading conditions can occur in the field when there are soil layers of different densities adjacent to each other. Susceptibility to flow liquefaction instability is determined not by the sign of β , but by the sign of \mathcal{L} . Depending on the imposed β_p , the sign of \mathcal{L} can change. Figure 2.3 shows how negative (or expansive) values of β_p increase \mathcal{L} , while positive (or contractive) values of β_p reduce \mathcal{L} . It just so happens that during undrained triaxial compression, since $\beta_p = 0$, the sign of β determines the sign of \mathcal{L} . Stable response of loose sands and unstable response of dense sands under proportional strain triaxial compression have been observed in experimental and numerical studies in the past [15, 19–22, 42, 80]. Note that $\mathcal{L} > 0$ signifies a potential to liquefy. It does not sufficiently imply occurrence of flow liquefaction. Sustained loading with $\mathcal{L} > 0$ is necessary for the soil to encounter flow liquefaction instability. Finally, note that $\mathcal{L} = 0$ implies that the imposed dilatancy β_p on the soil specimen is equal to the natural dilative tendency β of the assembly. If such a situation arises, the specimen will behave as if under drained triaxial compression, and pore pressure will not change.

2.4 Necessary precursor for onset of flow liquefaction instability

As mentioned in the introduction, the central objective of this paper is to investigate the origins of flow liquefaction instability. We do so by analyzing the phenomenon under proportional strain triaxial compression. We discussed that if $\mathcal{L} > 0$, then the imposed radial strain increment is more expansive than the drained radial strain increment, which has the effect of increasing the pore pressure. However, it is well known that rise in pore pressure is necessary but not sufficient to cause flow liquefaction instability. For instance, in the case of a dense sand subjected to undrained triaxial compression, pore pressure initially rises, but following phase transformation, $\mathcal{L} < 0$ and pore pressure falls. To address this issue, we now analyze the stress evolution during proportional strain triaxial compression and arrive at a nec-

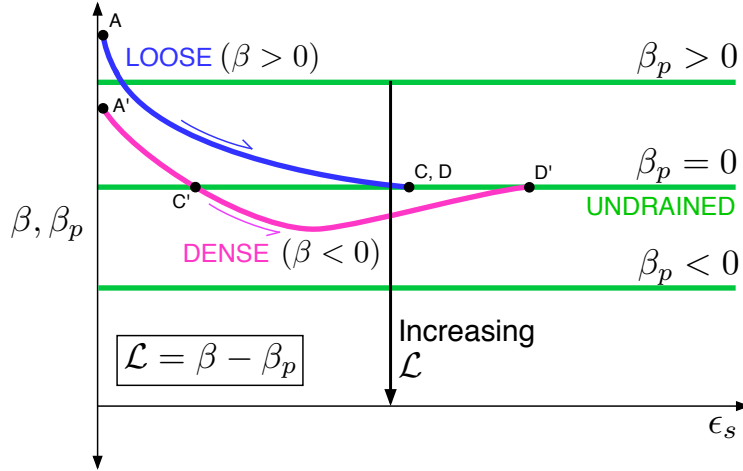


Figure 2.3: Dilative tendencies of loose and dense sand during drained triaxial compression. A = start, C = Phase Transformation, D = Critical state. The primes indicate similar stages for dense sand. $\beta > 0$ indicates contraction during drained triaxial compression, $\beta < 0$ indicates dilation during drained triaxial compression. Proportional strain triaxial compression imposes a volume change that is inconsistent with the natural dilative tendency. If $\beta_p = 0$, a loose soil is susceptible to flow liquefaction while a dense soil exhibits stable behavior. For $\beta_p < 0$, even a dense soil can become susceptible to flow liquefaction. For $\beta_p > 0$, even a loose soil can exhibit stable behavior.

essary precursor for the origin of flow liquefaction instability. This provides further insight into the mechanics of origin of flow liquefaction instability under proportional strain triaxial compression. We first consider the special case of an undrained triaxial compression test, for which the onset of flow liquefaction instability (equation 2.1) can be expressed as a function of *total* axial ($\dot{\sigma}_a$) and radial stress ($\dot{\sigma}_r$) increments, as well as *effective* axial ($\dot{\sigma}'_a$) and radial stress ($\dot{\sigma}'_r$) increments:

$$\dot{q} < 0 \quad \Rightarrow \quad \dot{\sigma}_a - \dot{\sigma}_r < 0 \quad \Rightarrow \quad \dot{\sigma}'_a - \dot{\sigma}'_r < 0 \quad (2.16)$$

Boundary condition imposes constant *total* radial stresses ($\dot{\sigma}_r = 0$). This implies:

$$\dot{\sigma}'_r = \dot{\sigma}_r - \dot{\theta} \quad \Rightarrow \quad \boxed{\dot{\sigma}'_r = -\dot{\theta}} \quad (2.17)$$

where $\dot{\theta}$ is the pore pressure increment. The instability criterion can now be expressed as:

$$\dot{\sigma}'_a + \dot{\theta} < 0 \quad (2.18)$$

Note that $\mathcal{L} > 0$ implies $\dot{\theta} > 0$. Therefore, we need $\dot{\sigma}'_a < 0$ to satisfy the above equation. We now arrive at a *necessary precursor for flow liquefaction instability*

during undrained triaxial compression:

$$\boxed{\dot{\sigma}'_a < 0} \quad (2.19)$$

Equation 2.19 suggests that during an undrained triaxial compression test, a soil specimen may encounter flow liquefaction instability only if it is undergoing a reduction in effective axial stress, hereby referred to as axial softening. Prevalence of axial softening prior to onset of instability has been documented in the past [21].

Remark 1: It must be noted that equation 2.19 by itself is necessary but not a sufficient condition for flow liquefaction instability under proportional strain triaxial compression. It is possible for the assembly to be softening axially, yet still be stable. As long as $\dot{q} > 0$, an assembly will be stable despite axial softening. Onset of axial softening can be thought of as a warning sign. If the same loading is applied continuously (sufficiency condition) despite axial softening (necessity condition), then as long as $\mathcal{L} > 0$, pore pressure will continue to rise and onset of instability is inevitable. If loading conditions are changed such that $\mathcal{L} < 0$, pore pressure will drop and the soil will exhibit stable behavior. Also, note that in this context, axial softening should not be confused with the vanishing of hardening modulus as in elasto-plasticity theory.

Remark 2: It must also be noted that not all soils are capable of existing in liquefiable states. Clays, for instance, are inherently non-liquefiable [44]. Axial softening in clays should not be taken as a precursor to flow liquefaction instability. Care must be taken to ensure that the soil in question satisfies the compositional criteria [44] that make it capable of existing in a liquefiable state.

Geometrical argument for necessity of $\dot{\sigma}'_a < 0$

To get a more geometrical perspective of equation 2.19, we refer to Figure 2.4a that shows the evolution of various stress parameters, when a sand is subjected to undrained triaxial compression such that $\mathcal{L} > 0$. Note that for $\dot{q} = 0$, we need $\dot{\sigma}'_a = \dot{\sigma}'_r$. This means that we need the slopes of σ'_a and σ'_r to be equal. From equation 2.17, we know that the slope of σ'_r is always negative. Therefore, the only way the two slopes can be equal is if the slope of σ'_a becomes negative at some point.

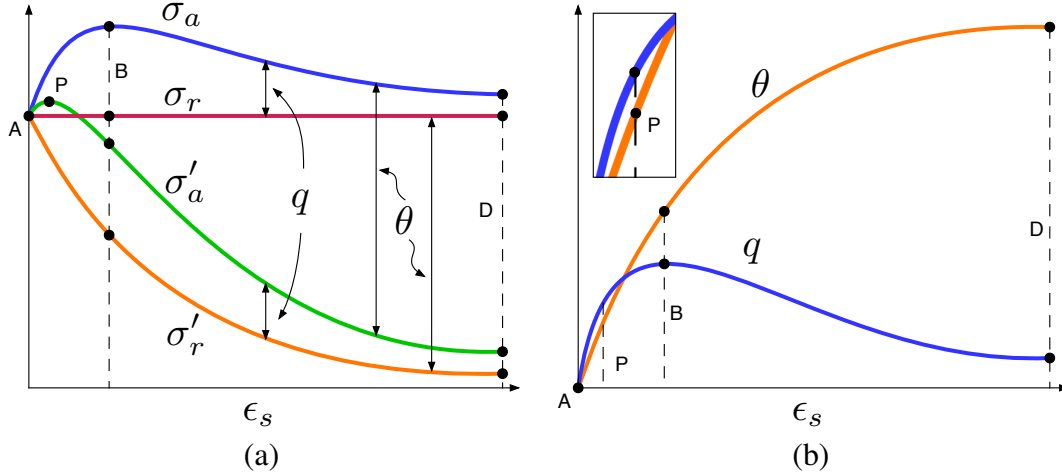


Figure 2.4: Undrained triaxial compression behavior when $\mathcal{L} > 0$. A = start, P = Precursor to instability ($\dot{q} \leq \dot{\theta}$, $\dot{\sigma}'_a \leq 0$), B = Instability, D = Critical State. (a) Evolution of total and effective axial and radial stresses. Before P: $\dot{\sigma}'_a > 0$. After P: $\dot{\sigma}'_a < 0$. (b) Evolution of deviatoric invariant q and pore pressure θ . Before P: $\dot{q} > \dot{\theta}$. After P: $\dot{q} < \dot{\theta}$.

Extension to proportional strain triaxial compression test

As mentioned earlier, some investigators [19, 20, 22, 42] prefer the use of an alternate response variable to mark the onset of instability for a proportional strain triaxial test. The alternate response variable can be expressed as $\xi = \sigma'_a + 2\alpha_p\sigma'_r$ such that $\dot{\xi} = 0$ coincides with the loss of second order work and marks the onset of flow liquefaction instability; here $\alpha_p < 0$ and is defined in section 2.3. Under undrained conditions, ξ reduces to q . Since the total radial stress is constant, $\dot{\sigma}'_r = -\dot{\theta}$ and it can be easily shown that even for $\dot{\xi} < 0$ to be true, $\dot{\sigma}'_a < 0$ is a necessary precursor. Therefore, $\dot{\sigma}'_a < 0$ is a necessary precursor for onset of flow liquefaction stability in a proportional strain triaxial compression test.

Excess pore pressures

Since $\dot{\sigma}_r = 0$, we get $\dot{q} = \dot{\sigma}'_a$. We can thus express $\dot{\sigma}'_a$ as:

$$\dot{\sigma}'_a = \dot{q} - \dot{\theta} \quad (2.20)$$

Axial softening ($\dot{\sigma}'_a < 0$) implies:

$$\boxed{\dot{q} < \dot{\theta}} \quad (2.21)$$

Equation 2.21 presents an alternative form of the necessary precursor for flow liquefaction instability under proportional strain triaxial compression. It suggests that

axial softening or loss of effective axial stress occurs when the pore pressure increment is greater than the increment in deviatoric strength (Figure 2.4b). Note that as long as $\dot{q} > \dot{\theta}$, pore pressure rise will be in check and there will be no axial softening. This can be also be seen in the experimental results of Castro [13]. Mathematically, equations 2.19 and 2.21 are equivalent. Also, note that while deriving equation 2.21 from equation 2.19, we did not make any assumptions about the imposed strain path. Therefore, equation 2.21 holds for any proportional strain path in a triaxial test, not just the isochoric (or undrained) strain path.

Discussion

We belabor the importance of equation 2.19 (or 2.21) with some historical perspective. We refer to Figure 2.4. In the past, liquefaction was analyzed at point D. Thereafter, the concept of flow liquefaction instability was defined whereby point B was thought to be crucial to understanding liquefaction. The instability concept has proven to be very useful and a lot of progress has been made in understanding the macro and micro mechanics at the onset of flow liquefaction instability [3, 19, 20, 22, 42, 66]. Now, we propose that significance should also be given to point P since attainment of point P is a necessary precursor for getting to point B, assuming the same loading is applied continuously (sufficiency condition). The concept of a precursor has potential to further improve our understanding of origin of flow liquefaction. For instance, equation 2.21 sheds some light on the stable behavior of soil when $\mathcal{L} < 0$ (such as dilative assemblies under undrained conditions). In such assemblies, pore pressures drop ($\dot{\theta} < 0$). Since the assembly continues to strengthen, $\dot{q} > \dot{\theta}$ is always true and the necessary precursor for onset of instability is not met.

Remark 3: Note that the proposed necessary precursor is only applicable under idealized condition of proportional strain triaxial compression. An understanding of the physics underlying the origin of flow liquefaction instability under idealized conditions provides us with motivation to look for precursors to instability under different loading conditions, such as soil subjected to constant deviator stress loading, or a soil under more complex and general field conditions. Such a concept could prove to be very useful while monitoring static liquefaction in the field such as slope stability and landslides.

Remark 4: Although Figure 2.4 assumes an isotropic initial state of stress, the result should apply to anisotropic initial state of stress as well, since no assump-

tions were made about the initial stress state. However, in the case of an anisotropic initial stress state, it is possible that the soil may be susceptible to spontaneous liquefaction, whereby there is a rapid drop in deviator stress at the onset of undrained or proportional strain loading (e.g. [80]). In such a case it may not be possible to detect the aforementioned precursors. Although equations 2.19 and 2.21 will still be satisfied, they may not be able to serve as precursors or warning signs.

2.5 DEM Simulations

The objective of this section is to present simulation results to support our analysis. To that effect, we performed discrete element method (DEM) simulations. DEM is a numerical model that describes the mechanics of an assembly of particles [17]. We'll first briefly describe the contact model and then describe our simulations.

Description of the contact model

Figure 2.5 shows the schematics of the model employed to describe the contact between two particles. The microscopic constants used in the simulations are summarized in table 2.1.

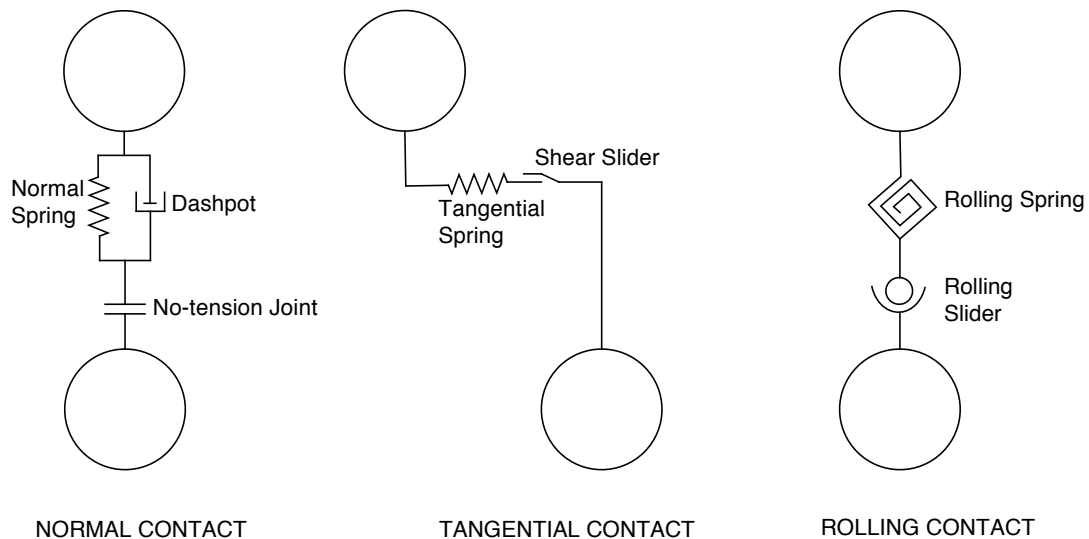


Figure 2.5: DEM contact model

The simulations were modeled after [29]. We employed the MechSys programming library to implement our DEM simulations.

Simulations

We simulated a polydisperse assembly of 1290 particles. The radii of the particles were uniformly distributed within a range of 0.05 to 0.5 cm. We simulated loose

Table 2.1: Microscopic constants used in the simulations.

Constant	Description
$K_n = 5000 \text{ kN/m}$	Contact normal stiffness
$K_t = 2500 \text{ kN/m}$	Contact tangential stiffness
$\mu = 0.3$	Microscopic friction coefficient
$G_n = 0.16 \text{ s}^{-1}$	Normal viscous coefficient
$G_t = 0.0 \text{ s}^{-1}$	Tangential viscous coefficient
$\xi = 0.12$	Rolling resistance stiffness
$\eta = 1.0$	Plastic moment coefficient

assemblies and dense assemblies. All assemblies were prepared by subjecting a virgin assembly to isotropic consolidation under drained conditions. Loose assemblies were obtained by isotropically consolidating an assembly to 100 kPa. Dense assemblies were obtained by isotropically consolidating an assembly to 700 kPa and then unloading it back to 100 kPa (giving us an over-consolidated assembly). All tests were conducted using dry spheres. Drained triaxial compression conditions were approximated by imposing a constant total radial stress ($\sigma_r = 100 \text{ kPa}$), and subjecting the assembly to axial strain increments. Proportional strain triaxial compression conditions were simulated by subjecting the assembly to an imposed dilatancy β_p , wherein the radial strain increment is proportional to the axial strain increment. Equivalent pore pressures were inferred using equation 2.17.

Results

Figure 2.6 shows the stress-path of ‘loose’ and ‘dense’ soil under drained and undrained triaxial compression conditions. Undrained triaxial compression is a special case of proportional strain triaxial compression where the imposed dilatancy $\beta_p = 0$. As expected, under undrained triaxial compression, loose sands exhibit unstable behavior, whereas dense sands exhibit stable behavior.

In addition to undrained triaxial compression, we also simulated proportional strain triaxial compression tests with an imposed dilatancy of (i) $\beta_p = 0.6$, and (ii) $\beta_p = -0.43$. We verify that given the right conditions, a loose soil that liquefies under undrained triaxial compression, may be stable under proportional strain triaxial compression. Conversely, a dense soil that is stable under undrained triaxial compression may liquefy under proportional strain triaxial compression. Figure 2.7

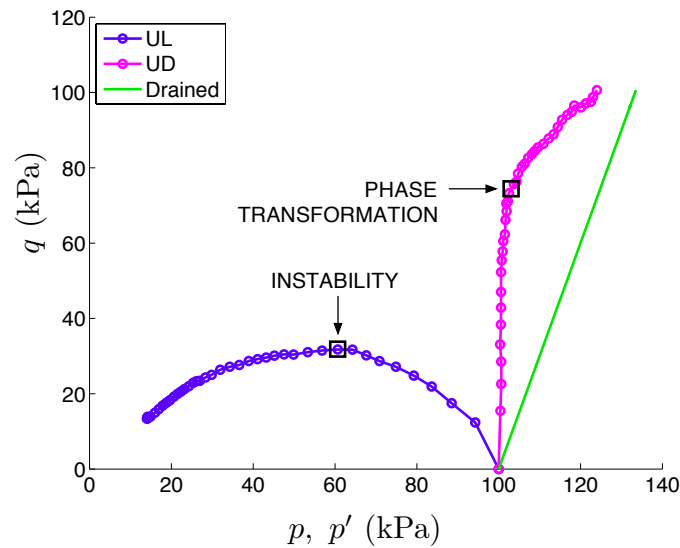


Figure 2.6: Evolution of stresses in the four sets of assemblies. UL: undrained loose, UD: undrained dense. Note the occurrence of instability and phase transformation in the UL and UD assemblies respectively.

shows the volume change or natural dilative tendency β of the ‘loose’ and ‘dense’ assemblies under drained triaxial compression. In addition, it also shows the imposed dilatancy β_p during proportional strain triaxial tests. Note that for $\beta_p = 0.6$, the flow liquefaction potential \mathcal{L} reduces for both loose and dense assemblies. Conversely, for $\beta = -0.43$, \mathcal{L} increases for both assemblies. The imposed dilatancy line forms a datum from which one can determine \mathcal{L} . If $\mathcal{L} > 0$, pore pressures rise. If $\mathcal{L} < 0$, pore pressures drop. Figure 2.7 also shows that the loose sample has a much higher susceptibility for liquefaction, something well known from experimental observations, but that can be clearly quantified by measuring the dilatancy inconsistency $\beta - \beta_p$, which we call the flow liquefaction potential \mathcal{L} . \mathcal{L} helps to visualize how a dense sample can become susceptible to liquefaction, and how a loose sample can exhibit stable behavior.

Figure 2.8 shows the behavior of ‘loose’ and ‘dense’ assemblies under proportional strain triaxial compression. As expected from Figure 2.7, $\beta_p = 0.6$ stabilizes the assemblies, while $\beta_p = -0.43$ makes them unstable.

Finally, we demonstrate the plausibility of axial softening (or reduction of effective axial stress) as a necessary precursor for onset of instability. Figure 2.9 shows the evolution of total and effective axial and radial stresses for an unstable assembly.

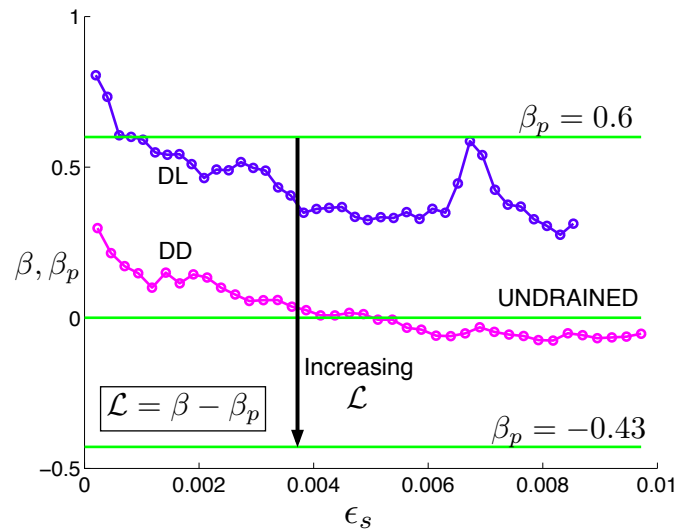


Figure 2.7: Natural dilatancy (β) in loose and dense assemblies vs imposed dilatancy (β_p). DL: drained loose, DD: drained dense. Note the inconsistency of β_p with β . For $\beta_p = 0.6$, the flow liquefaction potential \mathcal{L} reduces for both loose and dense assemblies. Conversely, for $\beta = -0.43$, \mathcal{L} increases for both assemblies. The imposed dilatancy line forms a datum from which one can determine \mathcal{L} . If $\mathcal{L} > 0$, pore pressures rise, making an assembly susceptible to flow liquefaction. If $\mathcal{L} < 0$, pore pressures drop and the assembly exhibits stable behavior. We also see that the loose sample has a higher susceptibility to flow liquefaction.

In this case, it is a loose assembly under undrained conditions. Figure 2.10 shows likewise for a stable assembly, in this case, a dense assembly under undrained conditions. Note the occurrence of axial softening in the unstable assembly (Figure 2.9a) and lack of it in the stable assembly (Figure 2.10a). Applying the same loading continuously (sufficiency condition) caused the assembly in Figure 2.9 to experience flow liquefaction. The stress evolution in Figures 2.9 and 2.10 occur for any stable/unstable assembly under proportional strain triaxial compression. For instance, a dense assembly that is unstable (for example, if $\beta_p = -0.43$) has stress evolution corresponding to Figure 2.9. A loose assembly that is stable (for example, if $\beta_p = 0.6$) has stress evolution corresponding to Figure 2.10. Furthermore, Figures 2.9b and 2.10b show the clear difference that induces liquefaction in unstable sands and not in stable sands. It is clear that the increment of pore pressures becomes greater than the increment of shear strength at point P, which marks the onset of axial softening as a necessary condition for liquefaction. In stable samples, such as that shown in Figure 2.10, pore pressures rise initially, but not at a rate sufficiently high to provoke axial softening. Note that we have presented simulations only for

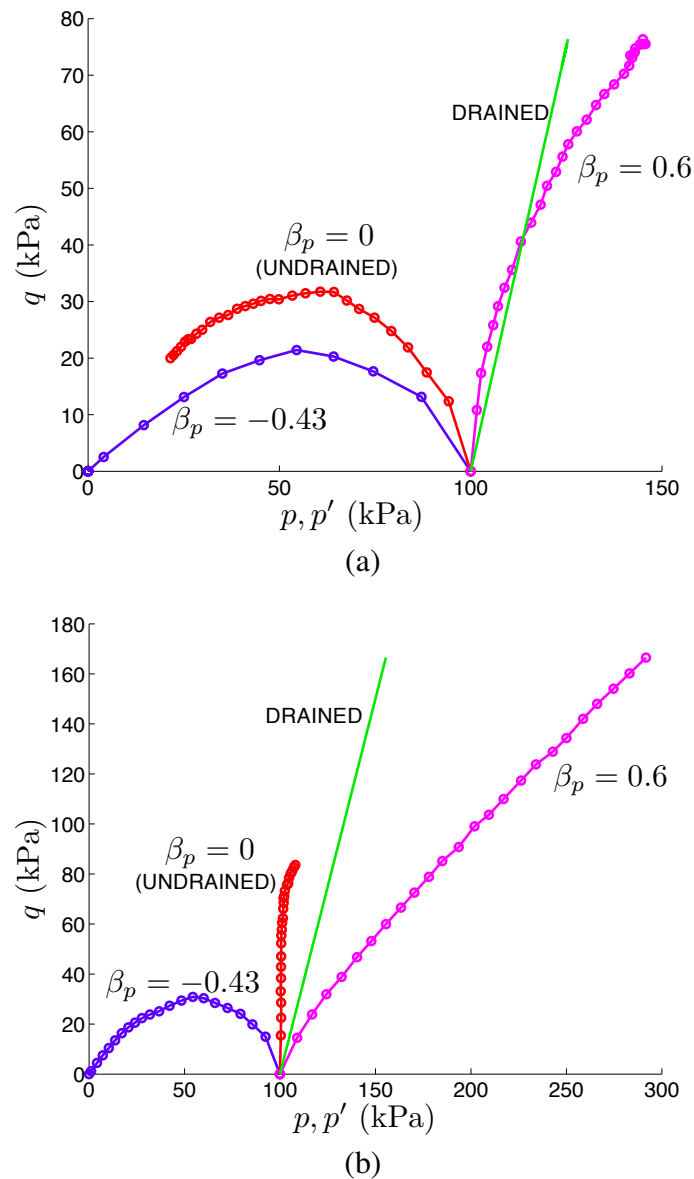
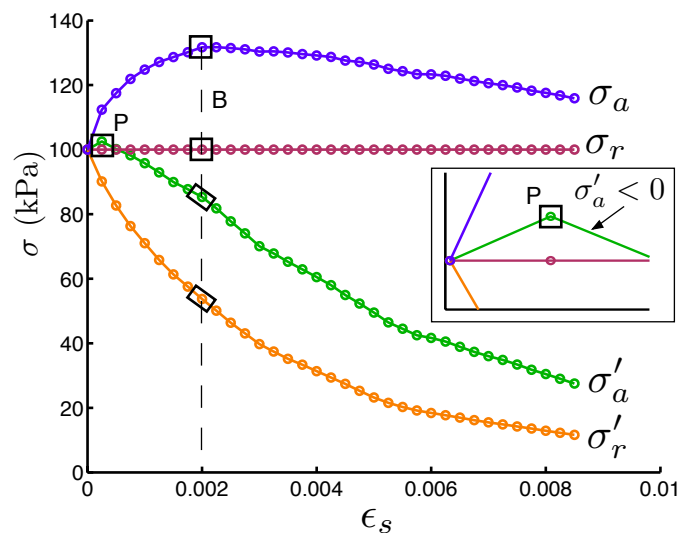


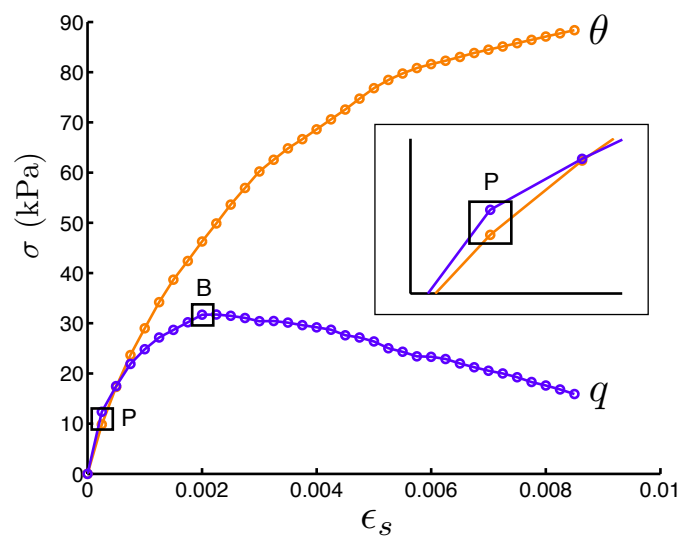
Figure 2.8: Evolution of stresses under proportional strain triaxial compression. (a) Loose assembly. (b) Dense assembly. Note how $\beta_p = 0.6$ stabilizes the assemblies, while $\beta_p = -0.43$ makes them unstable.

samples with an isotropic initial state of stress. Although our theoretical analysis did not make any assumptions about the initial state, behavior of samples with different initial conditions must still be verified experimentally or numerically.

Remark 5: For the simulation shown in Figure 2.9, axial softening occurs at about 10% of the strain needed for onset of flow liquefaction instability. This shows why



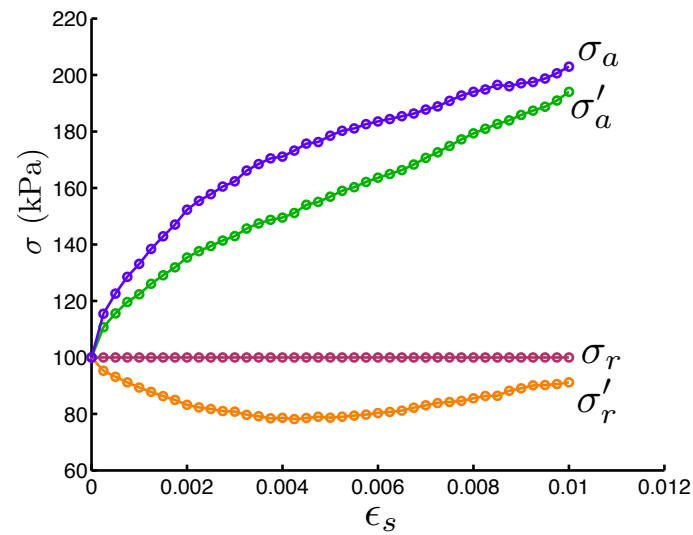
(a)



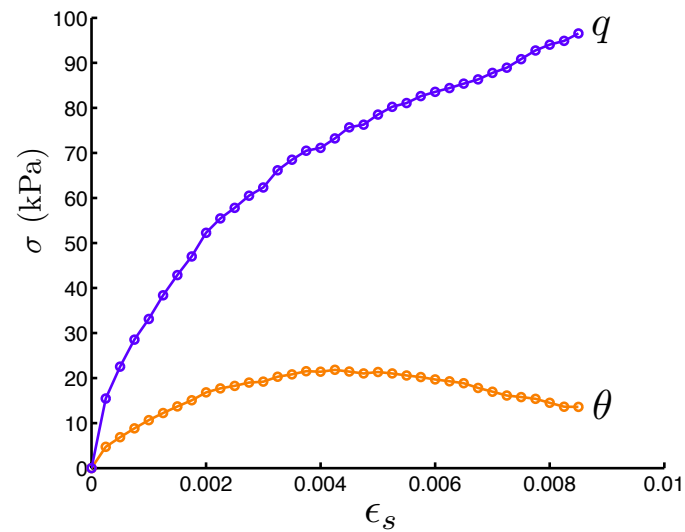
(b)

Figure 2.9: (a) Axial and radial effective and total stresses in an unstable assembly, in this case, loose assembly under undrained triaxial compression. Note the occurrence of axial softening (see inset corresponding to point P) and subsequent instability (B). At instability, note that $\dot{\sigma}'_a = \dot{\sigma}'_r$ and $\dot{\sigma}_a = \dot{\sigma}_r$. (b) Evolution of deviatoric invariant q and pore pressure θ . Before P: $\dot{q} > \dot{\theta}$. After P: $\dot{q} < \dot{\theta}$ (see inset corresponding to point P).

the concept of a necessary precursor is a powerful tool. If the necessary precursor is met, and the same loading is applied continuously (sufficiency condition), then the soil will experience flow liquefaction. This provides us with motivation to investigate and look for necessary precursors under different initial and loading



(a)



(b)

Figure 2.10: (a) Axial and radial effective and total stresses in a stable assembly, in this case, dense assembly under undrained triaxial compression. Note that there is no axial softening and the assembly continues to strengthen. (b) Evolution of deviatoric invariant q and pore pressure θ . Note that $\dot{q} > \dot{\theta}$ at all times.

conditions. Such a concept could prove to be very useful while monitoring static liquefaction in the field such as slope stability and landslides. If a soil is deemed “at risk” (via some as yet undetermined precursor for field conditions), it could be monitored and steps be taken to mitigate the effects of the instability.

2.6 Conclusions

We defined a new flow liquefaction potential \mathcal{L} for determining flow liquefaction susceptibility during proportional strain triaxial compression. The potential is a function of inconsistency between the natural dilative tendency β and the imposed dilatancy β_p , i.e., $\mathcal{L} = \beta - \beta_p$. If $\mathcal{L} > 0$, pore pressures rise, whereas if $\mathcal{L} < 0$, pore pressures drop. An analysis of \mathcal{L} provided us with a micro-mechanical interpretation of why given the right conditions, a loose soil that contracts during drained triaxial compression and liquefies under undrained triaxial compression, may be stable under proportional strain triaxial compression. Conversely, it also provided us with an interpretation of why a dense soil that dilates during drained triaxial compression and is stable under undrained triaxial compression, may liquefy under proportional strain triaxial compression. The undrained loose case is a special case of proportional strain triaxial compression (where $\beta_p = 0$), under which a soil can liquefy. Flow liquefaction criterion \mathcal{L} provides an elegant framework to visualize how a soil can liquefy despite volume changes; this can happen during seismic shaking in the field, or under static loading when there is differential pore pressure generation between adjacent soil layers with different densities. Unequal pore pressure generation can lead to pore water being injected into certain layers and being extracted from other layers, causing volume changes. Furthermore, since $\mathcal{L} > 0$ is necessary but not sufficient to induce flow liquefaction instability, we analyzed the stress evolution of proportional strain triaxial compression and investigated the mechanics of the test leading up to flow liquefaction instability. We arrived at reduction of effective axial stress (or axial softening) as a necessary precursor for flow liquefaction instability. Axial softening occurs when increment of pore pressure becomes greater than the increment of shear strength. In fact, for the simulation shown in Figure 2.9, axial softening occurs at about 10% of the strain needed for onset of flow liquefaction instability. This shows why the concept of a necessary precursor is a powerful tool. After attaining the precursor, the same loading must be applied continuously (sufficiency condition) for the soil to experience flow liquefaction. This provides us with motivation to investigate and look for necessary precursors under different initial and loading conditions. Such a concept could prove to be very useful while monitoring static liquefaction in the field such as slope stability and landslides. However, if the initial stress state of the soil is such that it is susceptible to spontaneous liquefaction, then the concept of a necessary precursor has limited applicability. Furthermore, care must be taken to ensure that the soil in question satisfies the compositional criteria needed to make it capable of

existing in a liquefiable state. For instance, clays are inherently non-liquefiable and will not exhibit liquefaction-like behavior even if they satisfy the necessary precursors. Lastly, note that the term ‘softening’ in this context should not be confused with the vanishing of hardening modulus as in elasto-plasticity theory.

In sum, the current work has taken some important steps towards understanding the mechanics of origin of flow liquefaction instability under proportional strain triaxial conditions. It complements the present understanding of the macro and micro-mechanics at the onset of flow liquefaction instability, and enables a deeper understanding of the phenomenon.